Applied Surface Science 255 (2009) 9712–9716

Contents lists available at ScienceDirect

Applied Surface Science

journal homepage: www.elsevier.com/locate/apsusc

Two-temperature relaxation and melting after absorption of femtosecond laser pulse

N.A. Inogamov [a,*], V.V. Zhakhovskii [b,c], S.I. Ashitkov [b], V.A. Khokhlov [a], Yu.V. Petrov [a], P.S. Komarov [b], M.B. Agranat [b], S.I. Anisimov [a], K. Nishihara [c]

[a] L.D. Landau Institute for Theoretical Physics RAS, Chernogolovka 142432, Russian Federation
[b] Joint Institute of High Temperature RAS, 13/19 Izhorskaya Street, Moscow 125412, Russian Federation
[c] Institute of Laser Engineering, Yamada-oka 2-6, Suita, Osaka 565-0871, Japan

ARTICLE INFO

Article history:
Available online 23 April 2009

PACS:
52.38.Mf
52.25.Os
02.70.Ns

Keywords:
Femtosecond laser ablation
Pump–probe
Optics of hot Al and Au

ABSTRACT

The theory and experiments concerned with the electron–ion thermal relaxation and melting of overheated crystal lattice constitute the subject of this paper. The physical model includes two-temperature (2T) equation of state, many-body interatomic potential, the electron–ion energy exchange, electron thermal conductivity, and optical properties of solid, liquid, and two phase solid–liquid mixture. Two-temperature hydrodynamics and molecular dynamics codes are used. An experimental setup with pump–probe technique is used to follow evolution of an irradiated target with a short time step 100 fs between the probe femtosecond laser pulses. Accuracy of measurements of reflection coefficient and phase of reflected probe light are 1% and ~ 1 nm, respectively. It is found that, *firstly*, the electron–electron collisions make a minor contribution to a light absorption in solid Al at moderate intensities; *secondly*, the phase shift of a reflected probe results from heating of ion subsystem and kinetics of melting of Al crystal during $0\,\text{ps} < t < 4$ ps, where t is time delay between the pump and probe pulses measured from the maximum of the pump; *thirdly*, the optical response of Au to a pump shows a marked contrast to that of Al on account of excitation of *d*-electrons.

1. Supersonic heating and melting

The three time slices "ei", m_1m_2, and c_1c_2 in Fig. 1 correspond to the following non-equilibrium processes: (e–i) the electron–ion thermal relaxation, (m) the melting of an overheated crystal lattice, and (c) the cavitation decay of a metastable state. The electron overheating ($T_e \gg T_i$) starts from ei_1 when a femtosecond laser pulse (fsLP) arrives [1–6] and disappears at ei_2 when temperatures T_e, T_i equilibrate ($t_{eq} = t_{ei2} = 3$–6 ps for Al at our intensities). It has been known that (i) for metals and semiconductors the fluences F near the ablation threshold F_{abl} are significantly higher than the melting threshold F_m [7], and (ii) the electronic heat conduction wave "EHC" in Fig. 2 is *supersonic* within the 2T slice "ei" shown in Fig. 1[3,5]. These facts (i and ii) result in the isochoric heating and stress confinement [1,4]. Estimates are: $x_{EHC} \sim \sqrt{\chi t}$, $\chi = lv/3$ is a thermal diffusivity, $l = v/\nu \sim 1$ nm is a mean free path, $\nu = 1/\tau$ is a collision frequency, v is the Fermi velocity. Therefore the Mach number of EHC wave is high $\dot{x}_{EHC}/c_s \sim 100\sqrt{\tau/t}$ up to a few picosecond. Within the time period $\sim t_{eq}$ the "EHC" creates a heated layer $d_T \approx 100$ nm thick in Al and ≈ 250 nm thick in Au [1,3–5]. The d_T is much thicker than acoustic penetration depth $c_s t$ at $t < t_{eq}$ as illustrated in Fig. 2. As a result of (i) and (ii) there is a volume non-equilibrium melting in the slice "m_1m_2" [1] with formation of overheated solid grains surrounded by melt. At the slice "m_2–fr" $t_{eq} < t <$ " fr" in Fig. 1 the heat wave velocity becomes much lower than c_s—and then the well-defined melting/recrystallization front is formed [1,4,8]. At $t =$ " fr" ~ 1 ns the melt layer covering a residue [9] of the target is solidified.

2. 2T hydrodynamics and light reflection

We use 2T hydrodynamical (2T-HD) equations [3–5,10–12] in Lagrangian variables x^0, t. For example, the equation for electron thermal energy is $\rho^0\partial(E_e/\rho)/\partial t = (\partial/\partial x^0)[(\rho\kappa/\rho^0)\partial T_e/\partial x^0] - p_e\partial u/\partial x^0 - (\rho^0/\rho)\alpha(T_e - T_i) + (\rho^0/\rho)Q$. The absorbed power is $Q(x,t) = [I(t)/\delta]\exp(-x/\delta)$, where δ is the thickness of the skin-layer shown in Fig. 2 as "skin". The pump intensity is I, ρ^0 is an initial density, E_e, E_i are the internal electron and ion energies, $\alpha(T_e - T_i)$ is the e–i energy exchange term. From the x-profiles ρ, f, T_e, T_i obtained by 2T-HD one can find the corresponding profile of the dielectric permittivity $\varepsilon(\rho, f, T_e, T_i) = \varepsilon_r + i\varepsilon_i$, where f is a volume fraction of the liquid phase in solid–liquid mixture. Next, for $\varepsilon(x,t)$ the Helmholtz equation $\partial^2F/\partial x^2 + \varepsilon(\omega/c)^2F = 0$, is solved for the amplitude F of the probe fsLP. Its solution gives the

* Corresponding author. Tel.: +7 495 7029317.
E-mail address: nailinogamov@googlemail.com (N.A. Inogamov).

0169-4332/$ – see front matter © 2009 Elsevier B.V. All rights reserved.
doi:10.1016/j.apsusc.2009.04.139

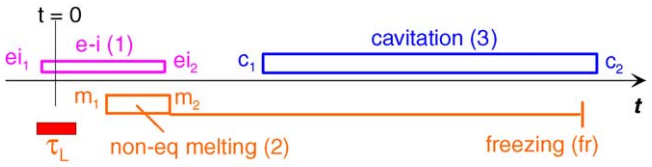

Fig. 1. The pump fsLP τ_L and a chain of kinetic or transient processes (1) "ei", (2) "m_1m_2", and (3) "c_1c_2" initiated by absorption of the pump.

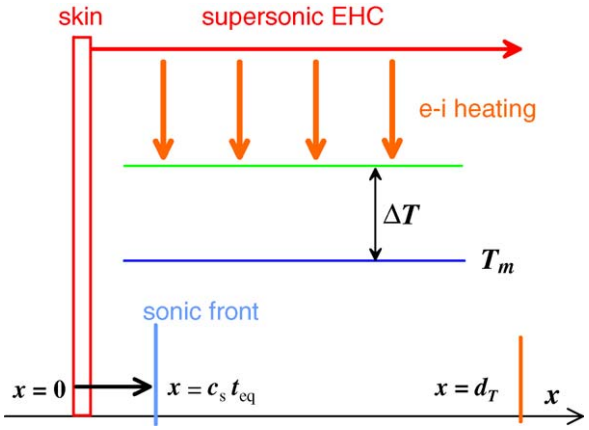

Fig. 2. Electrons are heated up by a pump in a skin layer of metal (the rectangular "skin"). The "EHC" supersonically (comp. the heat d_T and sonic propagations $c_s t_{eq}$ at $t = t_{eq}$) carries heat from the "skin" layer into the bulk of the target along the horizontal arrow (it shows the heat flux) forming the heated layer d_T. The energy of hot electrons is transferred to ions in fast process of "e–i heating" (the vertical arrows) [3]. As a result the crystal lattice is overheated to ΔT above the solidus temperature. The solidus and liquidus temperatures at ρ^0 are 1.2 kK, 1.48 kK (Al), 1.9 kK and 2.05 kK (Au). They are significantly higher than the melting or the triple point temperatures 933 K (Al) and 1337 K (Au) corresponding to melting at low pressure.

amplitude and phase of the reflected wave and correspondingly the time evolution $R(t), \psi(t)$ of the reflectivity R and phase ψ. They are compared with the experimental dependencies in Figs. 3 and 4 for Al. By contrast, the pump absorption is taken from the experiment [3]. In our experiments the chromium–forsterite laser with the pump $\lambda_{pump} = 1240$ nm and probe $\lambda_{prob} = 620$ nm is used [3,12]. A fsLP duration is 100 fs. Quantities R, ψ have been measured by microinterferometric technique [3,5,12,13].

3. 2T thermodynamics, collisions, and optics

The values $p_i, E_i(\rho, T_i)$ and $p_e, E_e(\rho, T_e)$ in 2T-HD are taken (as in [3]) from the wide-range equation of state [14] and Fermi model, $p = p_i + p_e$ is the total pressure. The coupling factor α and the heat capacity C_e are taken from [6]. According to the Drude formula the heat conductivity κ is

$$\kappa = \frac{(1/3)v^2 C_e}{\nu}, \qquad \nu_{ee} = b\left(\frac{E_F}{\hbar}\right)\left(\frac{T_e}{T_F}\right)^2, \tag{1}$$

$\nu = (\nu_{deg}^{-2} + \nu_{pl}^{-2})^{-1/2}$, $\nu_{deg} = (\nu_{ei} + \nu_{ee})(\rho/\rho^0)^{-1.3}$, $v = \sqrt{2E_F/m_e + 3k_B T_e/m_e}$, $E_F = k_B T_F$ is Fermi energy. At $T_e < T_F$ when electron degeneracy is significant the collision frequency is $\nu \approx \nu_{deg}$ ("deg" stands for degenerate). The electron–ion collisions ν_{ei} in ν_{deg} (1) is calculated separately for solid and liquid Al $\nu_{ei}^{sol} = 4.2 \times 10^{14}(T_i/934)$ (s^{-1}), $\nu_{ei}^{liq} = 1.1 \times 10^{14} T_i/(130 + 0.0367T_i - 66700/T_i)$ (s^{-1}), where T_i in K. The coefficients in ν_{ei}^{liq} approximate the quantum-mechanical MD κ of molten one-temperature (1T) Al [15].

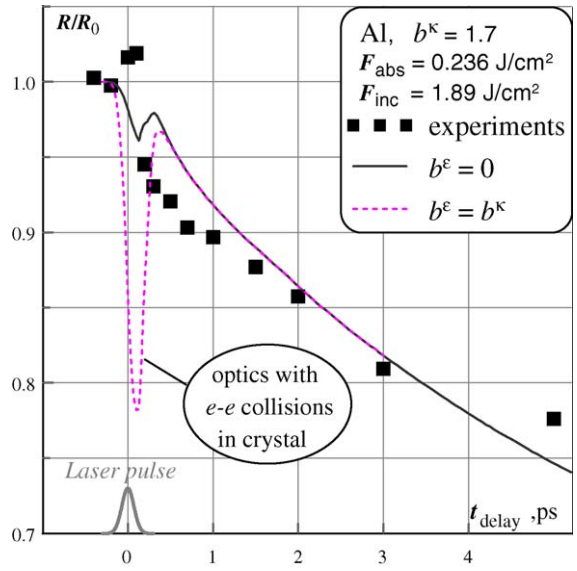

Fig. 3. Role of the e–e collision frequency ν_{ee} in optics. The solid curve is obtained for $\nu_{ee} = 0$. The experimental (squares) and theoretical reflectivity $R(t)$ normalized to initial R_0 of Al; $Z = 3$, $m_{eff}/m_e = 1.5$, Δ_{bb} from [16].

The value ε required for Helmholtz equation is a sum of the Drude and interband terms Δ_{bb} [2,12,16–18]

$$\varepsilon = 1 - \frac{(1 - i\nu/\omega)\omega_{pl}^2}{\omega^2 + \nu^2} + \Delta_{bb}, \qquad \omega_{pl}^2 = \frac{4\pi n_e e^2}{m_{eff}}, \tag{2}$$

In an Al crystal Δ_{bb} results from the transitions between parallel bands [16]. This term dominates at room temperatures. Its contribution increases the absorption more than by order of magnitude in comparison with pure Drude absorption. In a molten Al Δ_{bb} disappears [18]. A phenomenological dependence of Δ_{bb} on a total collision frequency ν has been proposed [16,2]. At large $\nu > \omega$ the term Δ_{bb} becomes small as compared to the Drude term as it is in liquid.

4. Role of ν_{ee} in optics

In an early stage the T_e is high—then the ν_{ee} (1) dominates in the total frequency ν (1). There are different coefficients b^κ and b^ε for the ν_{ee} (1) in expressions for κ (1) and for optics—in the Drude and

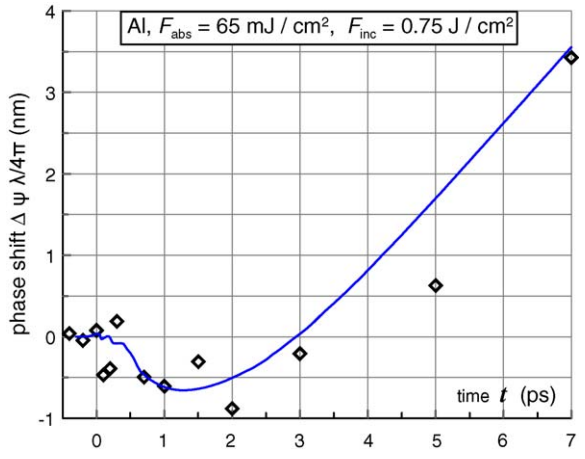

Fig. 4. The drop of the phase shift $\Delta\psi$ results from the solid–liquid transition within first few picoseconds, $\Delta\psi = \psi(t) - \psi_0$, ψ_0 is an initial phase (a phase of reflected wave from a cold target). Diamonds indicate experimental data.

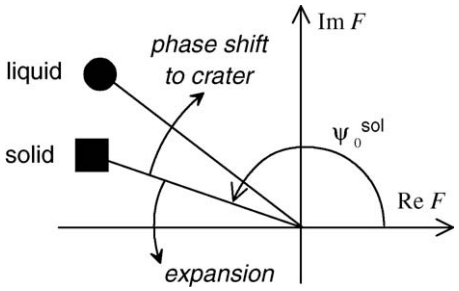

Fig. 5. Deviation of a phase of reflected light resulting from melting, F is a complex amplitude of a reflected wave. $\psi_0^{sol} = \pi - 12.5\,(\mathrm{nm})\,4\pi/\lambda_{prob}$ and $\psi_0^{liq} = \pi - 14.7\,(\mathrm{nm})\,4\pi/\lambda_{prob}$.

in the interband terms (2). In crystals the b^κ includes normal and Umklapp processes while the b^ε in the solid Al may differ from zero as a result of the Umklapp effect. In liquid $b^\varepsilon = 0$—the e–e collisions do not contribute into optical absorption as the Umklapp is impossible. In Al a Fermi sphere is larger than in Au while the Brillouin zones are approximately equal (the lattice constants are ≈ 0.4 nm for Al and Au both). Therefore the Umklapp effect is more significant in Al. Value of b in (1) is a subject of discussions. Below the Debye temperature the $\nu_{ei} \propto T^5$ tends to zero strongly and becomes less than the $\nu_{ee} \propto T^2$. Then specific electrical resistance $r = 1/\sigma$ for perfect crystals is $r = AT^2 + CT^5$. The measurements [19] give $b^\varepsilon = 15$. Here we suppose that ν_{ee} does not depend on frequency of electromagnetic field and the coefficient b in (1) for resistance r is equal to b^ε. By contrast, the theory [19] gives $b^\varepsilon = 0.6$. In [2] $b^\varepsilon = b^\kappa = 1$ is accepted. Performed optical measurements shown in Figs. 3 and 4 together with simulations give additional information about b^ε. The interesting sharp narrow "well" at the theoretical $R(t)$ in Fig. 3 corresponds to $b^\varepsilon = 1.7$. Its minimum is achieved when T_e and hence ν_{ee} (1) have the largest amplitudes (at the end of the pump). This well might be very useful for diagnostics. The left wing of the well follows the history of electron heating while the right wing reflects the kinetics of melting because the gradual phase transformation from crystal state to melt in a skin-layer progressively suppresses optical contribution of the e–e collisions (1). Unfortunately the well is not observed. Density of experimental points at the time axis in Figs. 3 and 4 is large enough to exclude missing of the well between the two successive points. The accuracy of experimental measurements of a relative reflection ($\approx 1\%$) is sufficient to catch the well. Analysis of our simulation runs in a fluence range $1 < F/F_{abl} < 4$ shows that it is necessary to have the b^ε below 0.2–0.5 to meet the measurements; for Al the calculated and measured thermomechanical ablation threshold is $F_{abl}|_{inc} = 0.75$ J/cm^2, $F_{abl}|_{abs} = 65$ mJ/cm^2[3].

5. Melting and decrease of phase angle

Simulations show that the phase evolution $\psi(t)$ presented in Fig. 4 contains important information concerning the kinetics of melting. The base for this is the difference commented in Fig. 5 between the defined in Section 4 ε^{sol} and ε^{liq}. As a result of attenuation of the band–band transition during melting the value $n = Re(N)$ becomes smaller. This is why the ψ_0^{liq} in Al is 2.2 nm differing from solid in the direction of the phase rotation to the crater. The value 2.2 nm corresponds to the case of a Fresnel reflection from homogeneous semispace. Remarkably that this small difference is measurable by the pump–probe interferometry. The phase $\Delta\psi(t)$ obtained from 2T-HD equations is compared with experimental data in Fig. 4. Expansion movement of reflecting boundary should increase $\Delta\psi$ but at the early time it decreases as a result of gradual melting of skin-layer. Agreement between

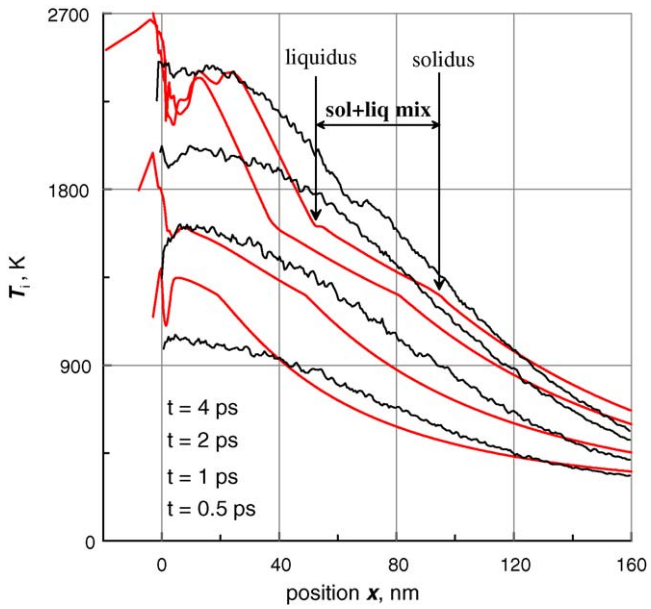

Fig. 6. Rise of T_i in 2T-HD and MD (the fluctuating profiles) simulations, Al, $F_{abs} = 65$ mJ/cm^2.

data and theory indicates that theory given below properly describes the melting.

Fig. 6 illustrates the heating of ions by hot electrons in 2T-HD model. In MD simulation atoms are heated by the space–time distributed thermostat power source with the temperature distribution taken from 2T-HD. This MD approach is similar to one developed in [1,20]. Particular mechanism of heating (heat flow from electrons or thermostat) has no action upon the kinetics of melting if we suppose that elastic moduli do not depend on T_e as in the case of Al [21]. In Fig. 6 the 2T-HD and MD T_i profiles are approximately the same. Some difference results from equilibrium and non-equilibrium description of melting. The arrows in Fig. 6 mark the slice of melting from equilibrium 2T-HD. The kinks at the ends of this slice result from hidden fusion energy. In MD the degradation of crystal symmetry during the fast heating and melting is distributed in wider range beyond the liquidus/solidus positions. Crystal beyond solidus is in overheated state [1,20].

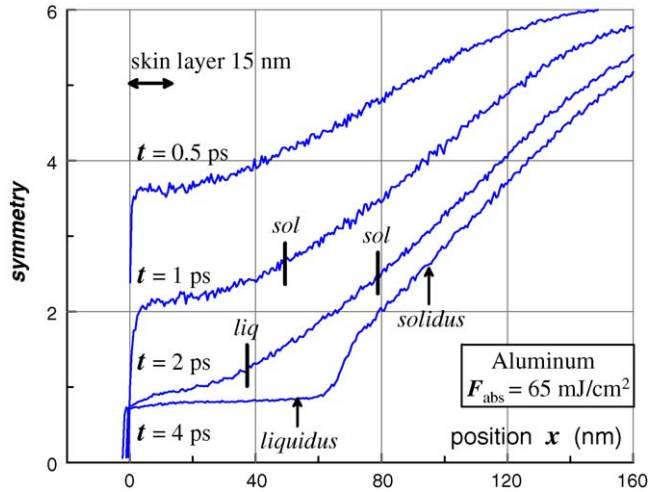

Fig. 7. Evolution of the phase composition as a result of the increase of T_i. The e–i heating gradually rises T_i as it is shown in Fig. 6. Transversally averaged s-profiles obtained from MD simulations are presented. The arrows "liquidus" and "solidus" at $t = 4$ ps are taken from Fig. 6. The values of the MD symmetry index $s(x,t) = 2.5$–2.7 taken at the 2T-HD solidus fronts are approximately the same for different instants.

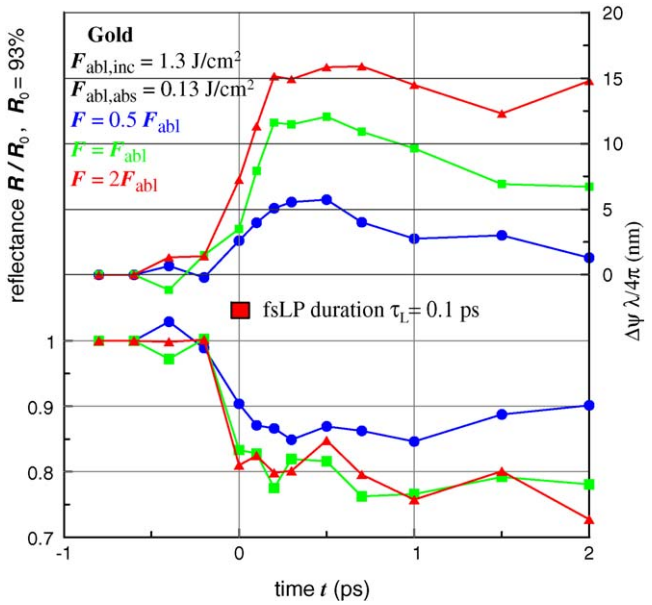

Fig. 8. Sharp change of R and ψ during pump action on bulk Au.

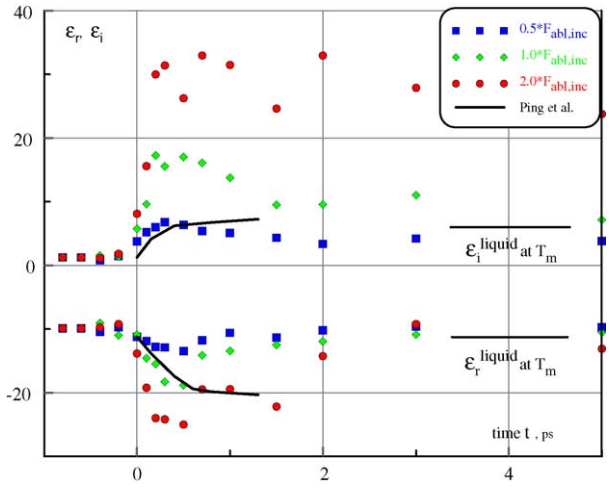

Fig. 9. Fast growth of ε as result of electron heating. The $\varepsilon = \varepsilon_r + i\varepsilon_i, \varepsilon_r < 0, \varepsilon_i > 0$ was calculated from data shown in Fig. 8 and the Fresnel formulae valid while the ε-profiles may be approximated by a step function. The solid curves presents data from [25] at $E_e = 2.9$ MJ/kg. They corresponds to our intermediate case $F_{inc} = F_{abl}$. Two bars give ε for liquid Au at 1337 K [18].

Phase transformation and propagation of melting into bulk is shown in Fig. 7. The profiles of the symmetry index s are presented. The index s is defined as a number of crystal axis passing through an atom and averaged over atoms within a x-slab, and $s = 6$ in a cold fcc lattice. One can see how quickly the rather thick (thicker than δ) layer of mixture is formed. Later the layer of pure melt (the plateau at the instant $t = 4$ ps at the s-profile in Fig. 7) appears. Much later the narrow melting front with small overheating separating a melt from a crystal is formed. Maximum thickness of the molten layer for the fluence $F_{abs} = 65$ mJ/cm^2 is $\approx$100 nm.

6. Gold optical response and *d*-electrons

Absorption of pump fsLP causes sharp changes in optical properties at very early time—during the pulse τ_L. They are shown in Fig. 8. This response is caused by fast heating of electrons. If we compare Figs. 3 and 4 (Al) and Fig. 8 (Au) having similar relative temperatures T_e/T_F at 2T stage and similar final $T_i = T_e$ temperatures after e–i relaxation we will see obvious large differences. They are related to the differences in the band structures of Al and Au [21]. Estimates of heating history from the maximum T_e to e–i thermalization give for the main seven thermal parameters $F_{inc}/F_{inc}|_{abl}$, F_{inc} (J/cm^2), F_{abs} (mJ/cm^2), $E_e|_{max}$ (MJ/kg), $T_e|_{max}$ (eV), $Z = N_{e6sp}$, $T_i|_{max}$ (kK) the values: (0.5, 0.7, 50, 1, 1.5, 1.2, 0.8), (1, 1.3, 140, 3, 2.5, 1.5, 2.5), (2, 2.9, 500, 10, 5, 2.4, 8) for the three cases shown in Figs. 8 and 9, where $F_{inc}|_{abl} = (1.3–1.4)$ J/cm^2 is a thermomechanical ablation threshold, $E_e|_{max}$, $T_e|_{max}$ are electron thermal energy and temperature at the end of a pump, Z is number of electrons exited from the d to the sp band at the maximum $T_e|_{max}$, $T_i|_{max}$ is maximum ion temperature achieved after e–i relaxation. An expression $E_e(T_e) = 45.7499T_e^2 - 119.756T_e^{2.1} + 105.419T_e^{2.2} - 30.9551T_e^{2.3}$ for electron thermal energy at fixed density $\rho = 19.3$ g/cm^3 approximates data obtained from the ABINIT [22] in the range $0.7 < T_e < 10$ eV, here E_e is in MJ/kg, and T_e in K. Experimental and theoretical values for the depth of a crater at a threshold $F_{inc}|_{abl}$ is 110 nm [5]. The first case with the smallest F_{inc} is near a melting threshold for bulk Au. Our three cases cover a range of energy densities obtained in [11,23–26] for 25–30 nm free-standing Au films.

The values of Z presented above have been defined using the ABINIT [22] code, the normalization condition for the number of electrons, and the expression for the amount of electrons in the sp band. The ABINIT has been used as in [21] for calculation of the T_e dependent DOS at different T_e supposing that density is equal to ρ^0 (isochoric heating). For given T_e the DOS of the d band obtained from ABINIT has been approximated by a rectangular and the DOS of the sp band has been described as the function $g(\epsilon) \propto \sqrt{\epsilon}$ in order to calculate Z. At a given T_e a root μ of the normalization condition:

$$11 = \frac{\sqrt{2}}{\pi^2}\frac{m_e^{3/2}}{\hbar^3}\frac{(k_B T_e)^{3/2}}{n_{atom}}\int_0^\infty \frac{\sqrt{x}\,dx}{e^{x-\mu/k_B T_e}+1} + L, \qquad (3)$$

where $L = (10/(E_1 - E_2))\ln((1 + e^{(\mu-E_1)/k_B T_e})/(1 + e^{(\mu-E_2)/k_B T_e}))$, defines a chemical potential $\mu(T_e)$, here E_1, E_2 are edges of the d band relative to the bottom point E_s of the sp bands. They are $\{E_1(T_e), E_2(T_e)\} = \{3.8, -1.8\}; \{3.5, -2\}; \{1.8, -3.2\}$ in eV; these three pairs correspond to $T_e = 1; 2;$ and 6 eV; the dependence of E_s on T_e is neglected in the estimates of Z. The first and the second terms correspond to the numbers of electrons in the sp and d bands, respectively. At room temperature these numbers are $Z = 1$ and 10. It is known that for Au difference between this approach and calculation of $\mu(T_e)$ with exact DOS is small [27]. The exact function $\mu(T_e)$ is obtained together with the DOS in the ABINIT simulation. The excitation degree Z is given by an expression $Z(T_e) = 11 - L$, where L stands for the second term in (3) but now with known $\mu(T_e)$.

The values of Z (for ω_{pl}) and collision frequency ν are necessary for the Drude estimates of ε. Growth of them is responsible for the rise of $|\varepsilon_r|, \varepsilon_i$ in Fig. 9. At room temperature ν/ω_{prob} is small: 1.2% from electrical and thermal conductivities or 3.3% from optical data [28], $\hbar\omega_{prob} = 2$ eV. Heating of electrons in our conditions enlarges ν to $\nu \sim \omega_{prob}$. There are three candidates responsible for the growth of ν : (i) an enhancement of ν_{ei} in solid Au with $T_e \gg T_i$ in comparison with $T_e = T_i$ (or 1T) case, (ii) ν_{ee} and Umklapps in crystal Au, and (iii) the e–e collisions between electrons from the d and the sp bands in solid or liquid Au. Let's consider them.

(i) For two (s and d) bands $\varepsilon = \varepsilon^s + \varepsilon^d$. ε^d is small because the number of holes in the d band is limited and holes are heavy $m^d/m^s \approx 5$. ε^s (2) depends on Z through ω_{pl} and on the collision frequency ν^s for s electrons. There is $\nu_{ei}^{sol}(T) = 1.2 \times 10^{11} T(s^{-1})$, $\nu_{ei}^{liq}(T) = 3.3 \times 10^{14} + 1.5 \times 10^{11} T$ for these electrons in 1T

gold [29], T in K. At $T_i = 1$–2 kK typical for Figs. 8 and 9 the enhancement of ν^s_{ei} (in comparison with room T) due to increase of T_i may be ~ 4. Melting can additionally enhance ν^s_{ei} from $\approx 2 \times 10^{14}$ to $\approx 5 \times 10^{14}$. But the time scale in Figs. 8 and 9 is short for melting in Au. T_e increase to 3–6 eV is not significant for the s band ν^s_{ei}. Therefore ν_{ei} remains small relative to ω_{probe} and cannot explain the sharp change of ε.

(ii) In Al ν^{umkl}_{ee} is small, Section 4. As was said, the Umklapp processes are weaker in Au as the result of smaller Fermi/Brillouin ratio. Therefore it seems plausible that this candidate is also unimportant.

(iii) Electrons from d versus sp bands have different angular momentum and effective mass. Therefore photons are absorbed in collisions between them. Corresponding frequency ν^{bb}_{ee} is given by (1) with possible dependence $b(T_e)$. The ν^{bb}_{ee} may be $\sim \omega_{prob}$ at $T_e \sim T_F$.

From imaginary and real parts of Eq. (2) we obtain $\hat{\nu} = \nu/\omega_{prob} = (\varepsilon_i - \Delta_i)/[1 - (\varepsilon_r - \Delta_r)]Z/m_{eff} = (1 + \hat{\nu}^2)(\varepsilon_i - \Delta_i)/20.6/\hat{\nu}$. The mass $m^{Au}_{eff}/m_e = 0.95$–1.15 at room temperatures [28] remains approximately the same with increase of T_e. This follows from our ABINIT simulations. According to [25] in 2T Au $E_d > \hbar\omega_{prob} = 2$ eV, where E_d is an absorption edge of the d-band. If we neglect the band–band term $\Delta_{bb} = \Delta_r + i\Delta_i$ in (2), $\Delta_r = 0$, $\Delta_i = 0$, then $(Z; \hat{\nu}) = (0.9; 0.5), (1.7; 0.9), (3.3; 1.3)$ at the maximum $|\varepsilon_r|, \varepsilon_i$ in the three cases shown in Fig. 9.

Our data shown in Fig. 9 agree with data from [25] in ε_r but give larger ε_i and have a maximum at the time dependence $|\varepsilon_r(t)|$ while the dependence $\varepsilon_r(t)$ from [25] saturates. Perhaps the last difference results from the conductive cooling absent in ultrathin films. Let's mention that data [25] contain the useful dependence $\varepsilon(\omega)$ but may be less accurate at a particular frequency. $(Z; \hat{\nu}) = (1.2; 0.4)$ for the maximum of the dependence $\varepsilon(t)$ from [25] shown in Fig. 9 as the solid curves. As a result of smaller ε_i these values are below than our values (1.7; 0.9) for the case with approximately the same energy E_e. Nevertheless there are appreciable excitation Z and frequent collisions. Therefore we can conclude that measurements confirm the theoretical findings presented above that a pump irradiation creates an excited population $(Z > 1)$ rising ω_{pl} (2) and transfers gold into the state with strongly collisional widened energy levels.

Acknowledgement

The work is supported by the RFBR Grant No. 07-02-00764.

References

[1] D.S. Ivanov, L.V. Zhigilei, Phys. Rev. B 68 (2003) 064114.
[2] D. Fisher, M. Fraenkel, Z. Henis, E. Moshe, S. Eliezer, Phys. Rev. E 65 (2001) 016409.
[3] S.I. Anisimov, N.A. Inogamov, Yu.V. Petrov, V.A. Khokhlov, V.V. Zhakhovskii, K. Nishihara, M.B. Agranat, S.I. Ashitkov, P.S. Komarov, Appl. Phys. A 92 (2008) 939.
[4] A. Volkov, L. Zhigilei, J. Phys.: Conf. Ser. 59 (2007) 640.
[5] N. Inogamov, V. Zhakhovskii, S. Ashitkov, Yu. Petrov, M. Agranat, S. Anisimov, K. Nishihara, V. Fortov, JETP 107 (2008) 1.
[6] Z. Lin, L. Zhigilei, V. Celli, Phys. Rev. B 77 (2008) 075133.
[7] A. Upadhyay, N. Inogamov, B. Rethfeld, H. Urbassek, Phys. Rev. B 78 (2008) 045437.
[8] W. Duff, L. Zhigilei, J. Phys.: Conf. Ser. 59 (2007) 413.
[9] The cavitation or run-away layer is thermally weakly coupled with a future crater bottom and therefore may remains molten while the bottom becomes frozen. At the c_1c_2 slice in Fig. 1 the cavitation layer is mechanically coupled with the bottom through the fragmentation or nucleation zone [3,5]. Agranat et al., Appl. Surf. Sci. 253 (2007) 6276.
[10] S.I. Anisimov, N.A. Inogamov, Y.V. Petrov, V.A. Khokhlov, V.V. Zhakhovskii, K. Nishihara, M.B. Agranat, S.I. Ashitkov, P.S. Komarov, Appl. Phys. A 92 (2008) 797.
[11] J. Colombier, P. Combis, E. Audouard, R. Stoian, Phys. Rev. E 77 (2008) 036409.
[12] M. Agranat, N. Andreev, S. Ashitkov, M. Veisman, P. Levashov, A. Ovchinnikov, D. Sitnikov, V. Fortov, K. Khichshenko, JETP Lett. 85 (2007) 271.
[13] V. Temnov, K. Sokolowski-Tinten, P. Zhou, D. von der Linde, J. Opt. Soc. Am. B 23 (2006) 1954.
[14] A.V. Bushman, G.I. Kanel', A.L. Ni, V.E. Fortov, Intense Dynamic Loading of Condensed Matter, Taylor & Francis Translation, 1993 295 pp.
[15] V. Recoules, J.-P. Crocombette, Phys. Rev. B 72 (2005) 104202.
[16] N.W. Ashcroft, K. Sturm, Phys. Rev. B 3 (6) (1971) 1898.
[17] E.D. Palik (Ed.), Handbook Opt. Const. Solids, Academic Press, NY, 1998.
[18] J.C. Miller, Philos. Mag. 20 (1969) 1115.
[19] M. Kaveh, N. Wiser, Adv. Phys. 33 (4) (1984) 257.
[20] Z. Lin, L.V. Zhigilei, J. Phys.: Conf. Ser. 59 (2007) 11.
[21] V. Recoules, J. Clerouin, G. Zerah, P. Anglade, S. Mazevet, Phys. Rev. Lett. 96 (2006) 055503.
[22] The ABINIT Code is a Common Project of the Universite Catholique de Louvain, Corning Inc., and Other Contributors (http://www.abinit.org).
[23] K. Widmann, T. Ao, M. Foord, D. Price, A. Ellis, P. Springer, A. Ng, Phys. Rev. Lett. 92 (2004) 125002.
[24] S. Mazevet, J. Clerouin, V. Recoules, P.M. Anglade, G. Zerah, Phys. Rev. Lett. 95 (2005) 085002.
[25] Y. Ping, D. Hanson, I. Koslow, T. Ogitsu, D. Prendergast, E. Schwegler, G. Collins, A. Ng, Phys. Rev. Lett. 96 (2006) 255003.
[26] T. Ao, Y. Ping, K. Widmann, D.F. Price, E. Lee, H. Tam, P.T. Springer, A. Ng, Phys. Rev. Lett. 96 (2006) 055001.
[27] Z. Lin, L.V. Zhigilei, Proc. SPIE 6261 (2006) 62610U.
[28] P.B. Johnson, R.W. Christy, Phys. Rev. B 6 (1972) 4370.
[29] I. Grigorév, E. Meilikhov, Phys. Values, Energoatomizdat, Moscow, 1991.